Supplementary Information

Hong-Liang Ye*[a], Kai-Jing Zhang*[b], Yuan-bin She*[c]

a. Innovation Laboratory for Sciences and Technologies of Energy Materials of Fujian Province (IKKEM) and College of Chemistry and Chemical Engineering, Xiamen University, Xiamen, Fujian 361005, China

b. CNPC EngineeringTechnology R&D Company Limited, Beijing 102206, China

c. College of Chemical Engineering, Zhejiang University of Technology, Hangzhou 310014, China

1. General Information

1.1 Chemicals and materials

4-Bromobenzaldehyde (98%), pyrrole (99%), anhydrous cobalt(II) acetate (98%), anhydrous manganese(II) acetate (98%), anhydrous copper(II) acetate (98%), anhydrous zinc(II) acetate (98%) and other metal acetates employed in syntheses of metalloporphyrins were purchased from Energy Chemical Co., Ltd., Shanghai Aladdin Biochemical Technology Co., Ltd., Adamas Reagent Co., Ltd., and Shanghai Macklin Biochemical Technology Co., Ltd., respectively. Tetraphenylmethane (96%), bromine (99%), tetrakis(triphenylphosphine)palladium (98%), anhydrous potassium carbonate (99%) and bis(pinacolato)diborane (99%) utilized in preparation of CoPor-PAFs were the commodities of Alfa Aesar, TCI, Meryer and Macklin respectively. 1-methyl-4-nitrobenzene (99%), ethylbenzene (99%), 1-ethyl-4-nitrobenzene (99%) and other alkyl aromatics employed as substrates in oxidation of benzylic secondary C–H bonds were purchased from Sinopharm Chemical Reagent Co., Ltd., J&K Scientific Co., Ltd., Aladdin Biochemical Technology Co., Ltd., Adamas Reagent Co., Ltd., and Macklin Biochemical Technology Co., Ltd., respectively. Aromatic alcohols and aromatic ketones in their highest purity available used as standard samples for qualitative and quantitative analyses were the commodities of above companies too. All the other general reagents were purchased from Sinopharm Chemical Reagent Co., Ltd., Hangzhou Shuanglin Chemical Reagent Co., Ltd., Shanghai Lingfeng Chemical Reagent Co., Ltd., and Guangdong Guanghua Sci-Tech Co., Ltd., respectively and used as received without any further purification.

1.2 Characterizations and instruments

The nuclear magnetic resonance (^{1}H NMR and ^{13}C NMR) spectra were collected on a Bruker AVANCE III (500MHz) spectrometer employing $CDCl_3$ as solvent and tetramethylsilane (TMS) as the internal standard at room temperature. The APCI-MS spectra were measured on an Agilent 6210 LC/TOF mass spectrometer equipped with atmospheric pressure chemical ionization source in the direct injection model. The Fourier transform infrared (FT-IR) spectra were obtained on a Thermo Nicolet 6700

spectrometer using KBr pellets. The X-ray photoelectron spectra (XPS) were collected on a Kratos AXIS Ultra DLD spectrometer to investigate the element species and their valence states in the obtained CoPor-PAFs. The scanning electron microscopy (SEM) images were recorded on a Zeiss Gemini 500 microscope to investigate the morphologies of the CoPor-PAFs. The transition electron microscopy (TEM) images were collected on a Hitachi HT 7700 microscope to investigate the morphologies of the CoPor-PAFs. The energy dispersive spectra (EDS) of the obtained CoPor-PAFs were recorded on an energy dispersive spectrometer coupled with the SEM and TEM analyses. The thermal gravimetric (TG) analyses were recorded on a PerkinElmer Diamond TG/DTA instrument from room temperature to 800 °C with the heating rate of 10 °C/min under air atmosphere. The X-ray diffraction (XRD) patterns were obtained on a PNAlytical X'Pert Pro X-ray diffractometer. The N_2 adsorption-desorption isotherms were collected on a Micromeritics ASAP 2460 instrument at -196 °C. Before measurement, the samples were degassed in vacuum at 150 °C for more than 10 h. The Brunauer-Emmett-Teller (BET) method was utilized to calculate the specific surface areas and the nonlocal density function theory was applied for the estimation of pore size, pore volume and pore distribution. The pore size distribution was determined using the NLDFT model. The electron paramagnetic resonance (EPR) spectra were recorded in the quartz tube on a JEOL JES-FA200 spectrometer at ambient temperature to investigate the free radical species in the catalytic system. And 5,5-dimethyl-1-pyrroline N-Oxide (DMPO) was employed as the radical trapping agent. The gas chromatographic (GC) analyses were performed on a Thermo Scientific Trace 1300 instrument with a TG-5MS capillary column (30 m × 0.32 mm × 0.25 μm) and a Flame Ionization Detector employing naphthalene as the internal standard. Both of the temperatures in the injector and detector were 250 °C. And the initial temperature of column was maintained at 60 °C for 1.0 min, and then increased to 250 °C in 10 °C/min, at which the temperature was kept for 10.0 min. The carrier gas was supplied by a nitrogen-hydrogen-air generator; the injection volume was 1.0 μL with a split ratio of 40:1.

2. Experimental Details

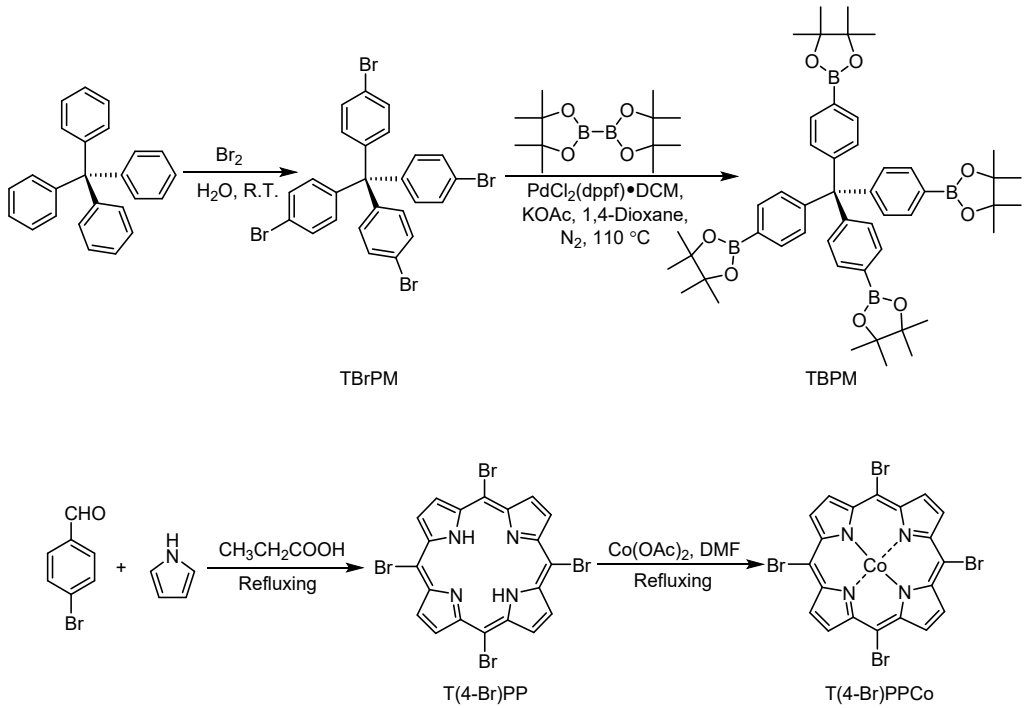

Scheme S1 The syntheses of TBPM and T(4-Br)PPCo.

2.1 Synthesis of tetrakis(4-bromophenyl)methane (TBrPM)

Tetrakis(4-bromophenyl)methane was synthesized through the procedure reported in literatures with some modifications as illustrated in **Scheme S1**[1, 2]. In the typical process, tetraphenylmethane (3.2044 g, 10.0 mmol) was dispersed in water (20 mL), and then liquid bromine (19.9763 g, 125.0 mmol) was added dropwise to the obtained mixture with intense stirring at room temperature in about 30.0 min. The resultant mixture was kept stirring at room temperature for 1.0 h. Then the obtained reaction mixture was cooled to 0 °C, and anhydrous ethanol (35 mL) was added slowly to dilute the reaction mixture. The precipitate collected through suction filtration was washed successively with 10% aqueous solution of NaOH twice (2×50 mL) and water twice (2×50 mL), and then recrystallized in the mixture of anhydrous ethanol (25 mL) and chloroform (25 mL) twice. After being dried at 90 °C for 8.0 h under reduced pressure, a pale yellow solid (3.4816 g) was obtained in the yield of 54.74%. ^{1}H NMR (500 MHz, $CDCl_3$): δ = 7.40 (d, 8H), 7.02 (d, 8H). ^{13}C NMR (125 MHz, $CDCl_3$): δ = 144.47,

132.39, 131.12, 120.84, 63.67.

2.2 Synthesis of tetrakis(4-(4,4,5,5-tetramethyl-1,3,2-dioxaborolan-2-yl)phenyl)methane(TBPM)

TBPM was synthesized through the procedure reported in literatures with some modifications as illustrated in **Scheme S1**[3, 4]. In the typical process, tetrakis(4-bromophenyl)methane (0.6360 g, 1.0 mmol), $PdCl_2$(dppf)•DCM (0.0817 g, 0.10 mmol), anhydrous potassium acetate (1.4721 g, 15.0 mmol) and 4, 4, 4', 4', 5, 5, 5', 5'-octamethyl-2, 2'-bi(1, 3, 2-dioxaborolane) (1.2697 g, 5.0 mmol) were dissolved in 1, 4-dioxane (20 mL) under atmosphere of nitrogen. The obtained reaction mixture was heated to 110 °C with vigorous stirring and kept stirring at 110 °C for 24.0 h. After being cooled down to room temperature, the solvent was evaporated under reduced pressure and the resultant solid was dissolved in dichloromethane (20 mL). The obtained solution was washed with water five times (5 × 20 mL) and dried on anhydrous sodium sulfate. The crude products were collected by evaporating the solvent under reduced pressure and subjected to the silica column chromatography for further purification employing the eluent of cyclohexane and dichloromethane ($V_{cyclohexane}$: $V_{dichloromethane}$ = 1 : 1). The target product was obtained through evaporating the solvent and drying at 90 °C for 8.0 h under reduced pressure as white power (0.3987 g) in the yield of 48.37%. ^{1}H NMR (500 MHz, $CDCl_3$): δ = 7.66 (d, 8H), 7.28 (d, 8H), 1.31 (s, 48H). ^{13}C NMR (125 MHz, $CDCl_3$): δ = 149.49, 134.14, 130.31, 83.73, 65.93, 24.87.

2.3 Synthesis of tetrakis(4-bromophenyl)porphyrin (T(4-Br)PP)

Tetrakis(4-bromophenyl)porphyrin (T(4-Br)PP) was synthesized through the Adler-Longo method with some modifications as illustrated in **Scheme S1**[5, 6]. Under the atmosphere of nitrogen, 4-bromobenzaldehyde (9.2510 g, 50.0 mmol) was dissolved in propionic acid (200 mL) and the resultant reaction mixture was heated to refluxing (145 °C) with stirring. When the reaction temperature reached, freshly distilled pyrrole (3.3545 g, 50.0 mmol) was injected into the reaction solution dropwise in about 15.0 min. The obtained solution was stirred under refluxing for 2.0 h and then

cooled down to room temperature. After standing at room temperature for 24.0 h, the crude product was collected through suction filtration under reduced pressure and suspended in methanol (300 mL) with stirring for 6.0 h at room temperature. By suction filtration, the collected precipitate was washed with methanol three times (3 × 100 mL) and subjected to the silica column chromatography successively for further purification employing the eluent of cyclohexane and dichloromethane ($V_{cyclohexane}$: $V_{dichloromethane}$ = 2 : 1). The target product was obtained through evaporating the solvent and drying at 80 °C for 8.0 h under reduced pressure as purple power (1.2485 g) in the yield of 10.74%.^{1}H NMR (500 MHz, $CDCl_3$): δ = 8.84 (s, 8H), 8.06 (d, 8H), 7.89 (d, 8H), -2.88 (s, 2H). ^{13}C NMR (125 MHz, $CDCl_3$): δ = 140.85, 135.84, 130.01, 122.67, 119.01. APCI-MS(m/z): 930.9 $[M+H]^+$.

2.4 Synthesis of tetrakis(4-bromophenyl)porphyrin cobalt (II) (T(4-Br)PPCo)

Tetrakis(4-bromophenyl)porphyrin cobalt (II) (T(4-Br)PPCo) was synthesized through the procedure in literatures with some modifications as illustrated in **Scheme S1**[5, 6]. Under the atmosphere of nitrogen, tetrakis(4-bromophenyl)porphyrin (0.9303 g, 1.0 mmol) and anhydrous cobalt (II) acetate (1.7702 g, 10.0 mmol) were dissolved in N, N-dimethylformamide (200 mL) and the obtained solution was heated to refluxing (abont 150 °C) with stirring. After stirring under refluxing for 24.0 h, the reaction mixture was cooled down to room temperature, and the solvent was removed through evaporation under the reduced pressure. The obtained solid was dissolved in dichloromethane (60 mL), and the resultant solution was washed with water five times (5 × 200 mL) until the upper layer became clear. The under layer was dried over anhydrous sodium sulfate. The crude products were collected by evaporating the solvent under reduced pressure and subjected to the silica column chromatography for further purification employing the eluent of cyclohexane and dichloromethane ($V_{cyclohexane}$: $V_{dichloromethane}$ = 1 : 1). The target product was obtained through evaporating the solvent and drying at 80 °C for 8.0 h under reduced pressure as reddish brown power (0.5598 g) in the yield of 56.70%. APCI-MS(m/z): 986.8 $[M]^+$.

2.5 Synthesis of CoPor-PAF-1

Under N_2 atmosphere, T(4-Br)PPCo (197.5 mg, 0.20 mmol), TBPM (164.9 mg, 0.20 mmol), and $Pd(PPh_3)_4$ (23.1 mg, 0.020 mmol) were dissolved in anhydrous 1,4-dioxane (16 mL). An aqueous solution of K_2CO_3 (221.1 mg, 1.6 mmol in 4 mL H_2O) was injected via syringe. The mixture was stirred at 110 ºC for 24 h under N_2. After cooling to RT, the precipitate was collected by suction filtration, washed sequentially with THF (50mL), $CHCl_3$ (50 mL), MeOH (50 mL), and H_2O (50 mL), then dried at 80 ºC under vacuum overnight to afford CoPor-PAF-1 as a reddish-brown powder (182.9 mg, 92.93%).

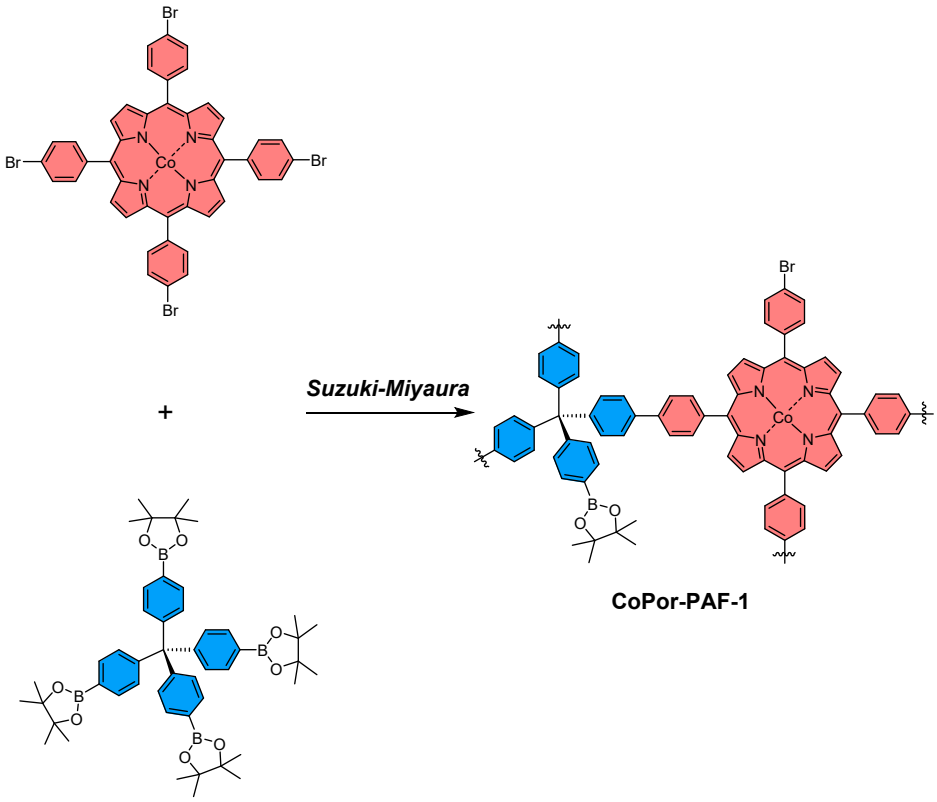

Scheme S2. The syntheses of CoPor-PAF-1

2.6 Synthesis of CoPor-PAF-2 and CoPor-PAF-3

The polymerization was performed as in Section 2.5 (24 h). Phenylboronic acid (97.5 mg, 0.80 mmol) in a 1,4-dioxane/H_2O (4:1, 5 mL) mixture was injected within 5 minutes, and stirring continued at 110 ºC for 24 h to cap residual Br groups. Workup

yielded CoPor-PAF-2 as a reddish-brown powder (179.8 mg, 91.35%).

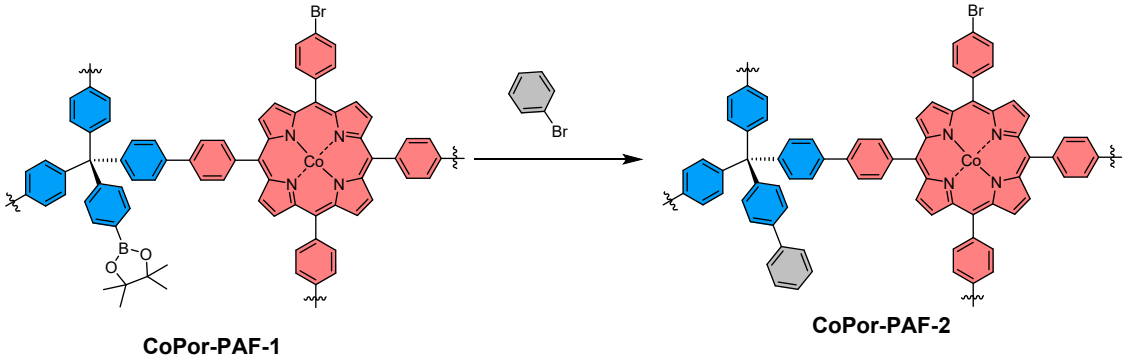

Scheme S3. The syntheses of CoPor-PAF-2

Note: CoPor-PAF-3 (174.9 mg, 88.9%) was synthesized similarly using bromobenzene (125.6 mg, 0.80 mmol) as the capping agent.

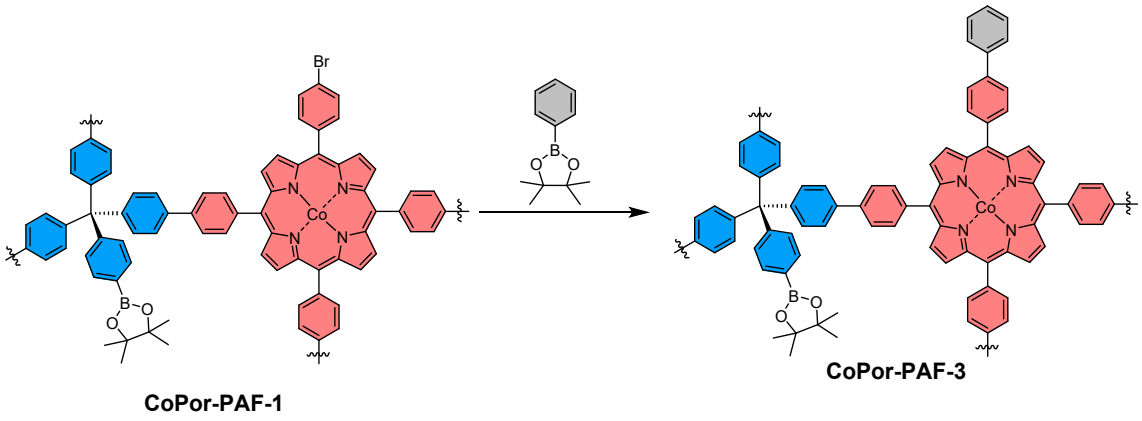

Scheme S4. The syntheses of CoPor-PAF-3

2.7 Synthesis of CoPor-PAF-4

After polymerization (Section 2.5, 24 h) and Br capping (phenylboronic acid pinacol ester, as in Section 2.6), bromobenzene (125.6 mg, 0.80 mmol) in a 1,4-dioxane/H_2O (4:1, 5 mL) mixture was injected within 5 minutes. The mixture was stirred at 110 ºC for 24 h to cap residual Bpin groups. Workup afforded CoPor-PAF-4 as a reddish-brown powder (126.8 mg, 64.43%).

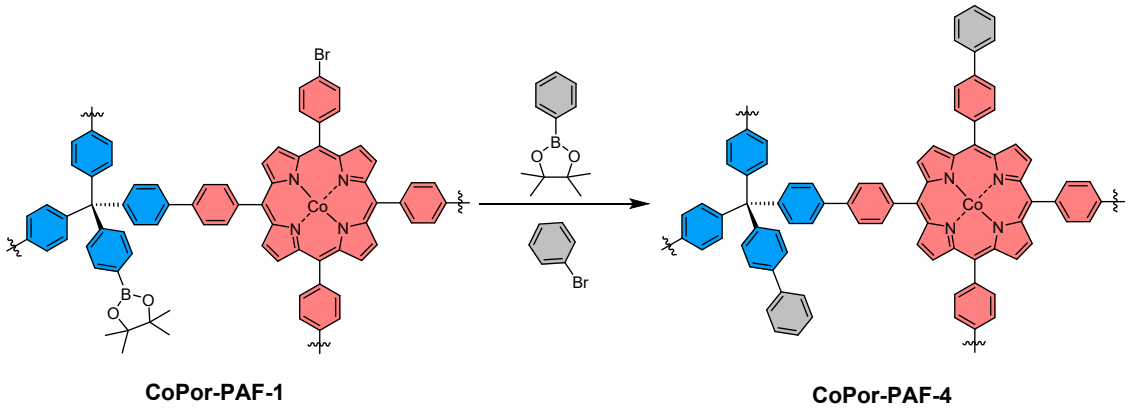

Scheme S5. The syntheses of CoPor-PAF-4

2.8 Solvent-Free catalytic oxidation of benzylic secondary C–H bonds with O_2

A measured quantity of CoPor-PAFs was suspended in an alkyl aromatic substrate (100 mmol) within the PTFE liner of a 100 mL autoclave. After sealing the reactor, the assembly was immersed in a temperature-controlled oil bath with magnetic stirring until reaching the target reaction temperature. At thermal equilibrium, oxygen was introduced to achieve specified system pressure. The gas feed line was equipped with a precision pressure regulator set to specified system pressure and held in the open position. This configuration allowed the reactor to be dynamically replenished with O_2 throughout the reaction, maintaining a constant total system pressure to compensate for consumption. The oxidative reaction was maintained under these conditions (fixed temperature/pressure) for predetermined durations. Post-reaction, the autoclave was immediately cooled to ambient temperature in an ice-water bath. Upon pressure release at 25 ºC, acetone (50 mL) was added to the crude mixture. Triphenylphosphine (2.6229 g, 10 mmol) was immediately added to decompose residual peroxides, followed by 30 minutes of agitation under ambient conditions. The quenched mixture was then metrically diluted to 100 mL with additional acetone. For quantitative gas chromatography (GC) analysis, an aliquot (10 mL) of the diluted solution was combined with naphthalene (0.1282 g, 1.0 mmol) serving as an internal standard. GC measurements determined substrate conversion and the selectivity towards aromatic

alcohol and ketone products.

2.9 Hydroperoxide analysis

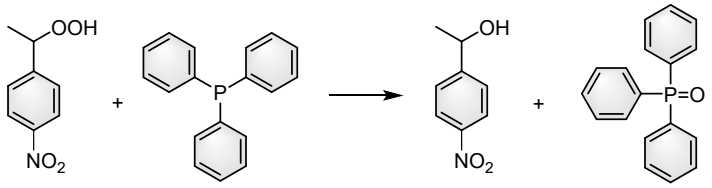

An aliquot of the crude reaction mixture was treated with an excess of PPh3. This step quantitatively reduces the hydroperoxide to the corresponding alcohol, simultaneously producing an equimolar amount of triphenylphosphine oxide ($POPh_3$). The amount of $POPh_3$ formed was then directly quantified using our standard gas chromatography (GC) method with an internal standard (naphthalene). Since the reduction is quantitative and the molar ratio is 1:1 (hydroperoxide : $POPh_3$), the molar percentage of the hydroperoxide in the original sample is directly equal to the molar percentage of $POPh_3$ measured. The amount of alcohol derived from the hydroperoxide is therefore also known from this value.

2.10 Electron paramagnetic resonance (EPR) analyses

CoPor-PAF-4 (5.0 mg, 0.05 mg/mmol) were dispersed in 1-ethyl-4-nitrobenzene (15.1170 g,100 mmol) in a high-pressure reactor (100 mL) equipped with a Teflon-lining. After sealing the reactor, the obtained reaction mixture was heated to 130 °C with stirring. O_2 was injected into the reactor to reach 1.0 MPa. The resultant reaction mixture was kept stirring at 130 °C and 1.0 MPa for 2.0 h and 4.0 h. The resultant reaction mixture (1 mL) was taken out from the sampling port, and 5,5-dimethyl-1-pyrroline N-Oxide (DMPO) (0.0011 g, 1×10^{-5} mmol) was added as the radical trapping agent to conduct the electron paramagnetic resonance (EPR) analyses on a JEOL JES-FA200 spectrometer at ambient temperature. The microwave frequency in EPR analyses was 9.26 GHz.

2.11 Free radical capture experiments

CoPor-PAF-4 (5.0 mg, 0.05 mg/mmol) and free radical capture reagent

(bromochloroform, *tert*-butyl bromide or diphenylamine, 5.0 mmol) were dispersed in 1-ethyl-4-nitrobenzene (15.1170 g, 100 mmol) in a high-pressure reactor (100 mL) equipped with a Teflon- lining. After sealing the reactor, the obtained reaction mixture was heated to 130 °C with stirring. O_2 was injected into the reactor to reach 1.0 MPa. The resultant reaction mixture was kept stirring at 130 °C and 1.0 MPa for 8.0 h, and cooled down to room temperature in ice water. When the reactor was opened, acetone (50 mL) was added to dilute the reaction mixture and triphenyl phosphine (2.6229 g, 10 mmol) was added immediately to transform the residual peroxide with stirring at room temperature for 30 min. The obtained reaction mixture was transferred to a 100 mL volumetric flask and diluted to 100 mL exactly using acetone as solvent. GC and GC-MS were employed to analyze the captured species, suppressed conversion and selectivity.

2.12 Isolation of hydroperoxide experiments

p-Ethylnitrobenzene (15.1170 g, 100 mmol) in a high-pressure reactor (100 mL) equipped with a Teflon- lining. After sealing the reactor, the obtained reaction mixture was heated to 130 °C with stirring. O_2 was injected into the reactor to reach 1.0 MPa. The resultant reaction mixture was kept stirring for 8.0 h. Post-reaction, the mixture was immediately subjected to a fast flash chromatography column at room temperature. The column was packed with silica gel and eluted using a mixture of dichloromethane and n-hexane. The collected fractions containing the target hydroperoxide were combined and concentrated under reduced pressure at low temperature to afford the isolated product, which was promptly analyzed by NMR spectroscopy.

2.13 Density Functional Theory (DFT)

All density functional theory (DFT) calculations were performed in the gas phase. Geometry optimizations and vibrational frequency calculations were conducted at the B3LYP/6-31G(d) level of theory, with the LANL2DZ effective core potential (ECP) and basis set used for cobalt (Co). Transition states were verified by intrinsic reaction coordinate (IRC) analysis.

3. Catalytic Oxidation Data

Table S1. Preliminary exploration on the metal active centers in oxidation of 1-ethyl-4-nitrobenzene[a].

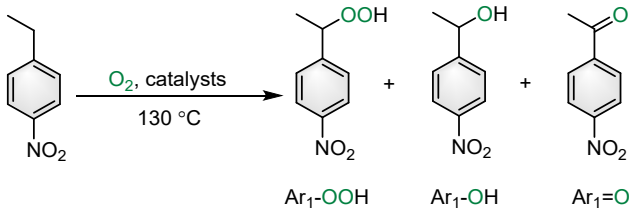

Entry	Catalysts	Conversion (%)	Selectivity (%)		
			Ar_1-OOH	Ar_1-OH	Ar_1=O
1	T(4-Br)PPCo	36.9	31.0	N. D.[b]	69.0
2	T(4-Br)PPMn	29.6	56.6	N. D.	43.4
3	T(4-Br)PPFe	22.4	69.7	N. D.	30.3
4	T(4-Br)PPCu	16.8	69.2	2.8	28.0
5	T(4-Br)PPNi	14.6	78.1	3.4	18.5
6	T(4-Br)PPZn	9.0	70.4	18.2	11.4

[a] *p*-ethylnitrobenzene (15.12 g, 100 mmol), catalyst (2.4×10^{-3}%, mol/mol), O_2 (1.0 MPa), 130 °C, 8.0 h, 600 rpm.

[b] No obvious product detected.

Table S2. Effect of CoPor-PAFs on oxidation of 1-ethyl-4-nitrobenzene[a].

Entry	Catalysts	Conversion (%)	Selectivity (%)		
			Ar_1-OOH	Ar_1-OH	Ar_1=O
1	CoPor-PAF-1	42.8	23.4	3.1	73.5
2	CoPor-PAF-2	39.7	27.6	3.2	69.2
3	CoPor-PAF-3	43.7	28.7	3.3	68.0
4	CoPor-PAF-4	52.2	16.6	1.7	81.7

[a] *p*-ethylnitrobenzene (15.12 g, 100 mmol), Catalysts (0.02 mg/mmol, 2.0 mg), O_2 (1.0 MPa), 130 °C, 8.0 h, 600 rpm.

[b] No obvious product detected.

Table S3. Effect of catalyst amount on oxidation of 1-ethyl-4-nitrobenzene[a].

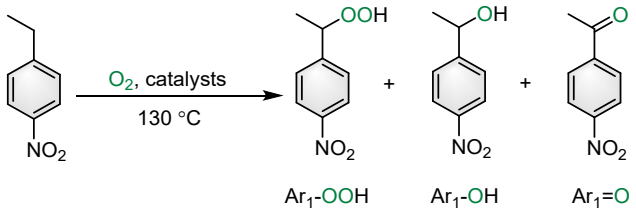

Entry	Catalyst amount (mg/mmol)	Conversion (%)	Selectivity (%)		
			Ar_1-OOH	Ar_1-OH	Ar_1=O
1[a]	Auto	9.6	69.0	13.0	18.0
1[b]	0.01	31.5	40.4	5.1	54.5
2[b]	0.02	42.8	23.4	3.1	73.5
3[b]	0.03	40.2	23.9	3.5	72.6
4[b]	0.04	N. D.[d]	N. D.	N. D.	N. D.
5[b]	0.05	N. D.	N. D.	N. D.	N. D.
6[b]	0.06	N. D.	N. D.	N. D.	N. D.
7[c]	0.01	37.4	34.7	6.8	58.5
8[c]	0.02	52.2	16.6	1.6	81.8
9[c]	0.03	53.2	9.9	2.2	87.9
10[c]	0.04	56.4	6.8	0.2	93.0
11[c]	**0.05**	**60.1**	**5.5**	**N. D.**	**94.5**
12[c]	0.06	60.7	5.3	0.3	94.4

[a] *p*-ethylnitrobenzene (15.12 g, 100 mmol), O_2 (1.0 MPa), 130 °C, 8.0 h, 600 rpm.

[b] CoPor-PAF-1 as catalyst.

[c] CoPor-PAF-4 as catalyst.

[d] No obvious product detected.

Table S4. Effect of reaction pressure on oxidation of 1-ethyl-4-nitrobenzene [a].

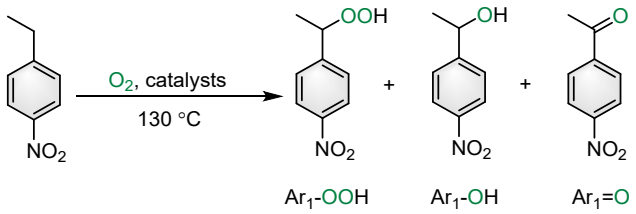

Entry	Pressure (MPa)	Conversion (%)	Selectivity (%)		
			Ar_1-OOH	Ar_1-OH	Ar_1=O
1	0.2	8.5	79.6	10.2	10.2
2	0.4	8.8	73.7	16.0	10.3
3	0.6	21.6	21.1	7.1	71.8
4	0.8	46.8	10.0	1.9	88.1
5	**1.0**	**60.1**	**5.5**	**N. D.**	**94.5**
6	1.2	61.3	5.1	0.6	94.3
7	1.4	61.1	4.9	0.3	94.8

[a] 1-Ethyl-4-nitrobenzene (15.12 g, 100 mmol), O_2, CoPor-PAF-4 (5.0 mg, 0.05 mg/mmol), 130 °C, 8.0 h, 600 rpm.

Table S5. Effect of reaction time on oxidation of 1-ethyl-4-nitrobenzene [a].

Entry	Reaction Time (h)	Conversion (%)	Selectivity (%)		
			Ar_1-OOH	Ar_1-OH	Ar_1=O
1	4.0	13.2	43.7	24.6	31.7
2	6.0	48.3	11.6	0.6	87.8
3	8.0	**60.1**	**5.5**	**N. D.**	**94.5**
4	10.0	62.0	3.3	0.4	96.3
5	12.0	63.2	3.1	0.5	96.4

[a] *p*-ethylnitrobenzene (15.12 g, 100 mmol), O_2 (1.0 MPa), CoPor-PAF-4 (5.0 mg, 0.05 mg/mmol), 130 °C, 600 rpm.

[b] No obvious product detected.

Table S6. Oxidation of benzylic secondary C–H bonds with O_2 catalyzed by Co-CoPor-PAF-4[a].

Entry	Substrate	Conversion (%)	Selectivity (%)		
			Ar_1-OOH	Ar_1-OH	Ar_1=O
1[b]	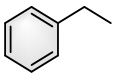	35.5	8.6	23.0	68.4
2	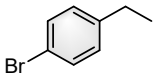	58.5	4.2	1.0	94.8
3[b]	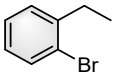	39.3	4.2	34.2	61.6
4	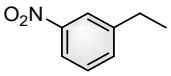	38.6	4.4	9.3	86.3
5[b]	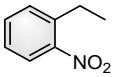	17.4	4.0	52.4	43.6
6[b]	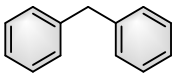	34.9	4.5	13.2	82.3
7	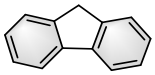	51.2	3.8	3.9	92.3
8[d]	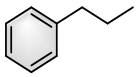	36.6	1.2	2.8	96.0
9[d,e]	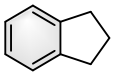	45.3	3.9	N. D.[c]	96.1
10[d,f]	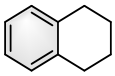	29.2	3.9	4.5	91.6
11[d]	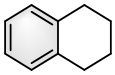	69.3	2.6	5.3	92.1
12[d]	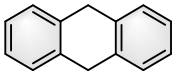	58.5	1.9	67.3	30.8
13[d]	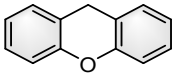	48.2	1.6	N. D.	98.4

[a] Substrate (100 mmol), O_2 (1.0 MPa), CoPor-PAF-4 (0.05 mg/mmol, 5.0 mg), 130 °C, 8.0 h, 600 rpm.

[b] 140 °C.

[c] No obvious product detected.

[d] O_2 (0.10 MPa)

[e] 110 °C.

[f] 120 °C.

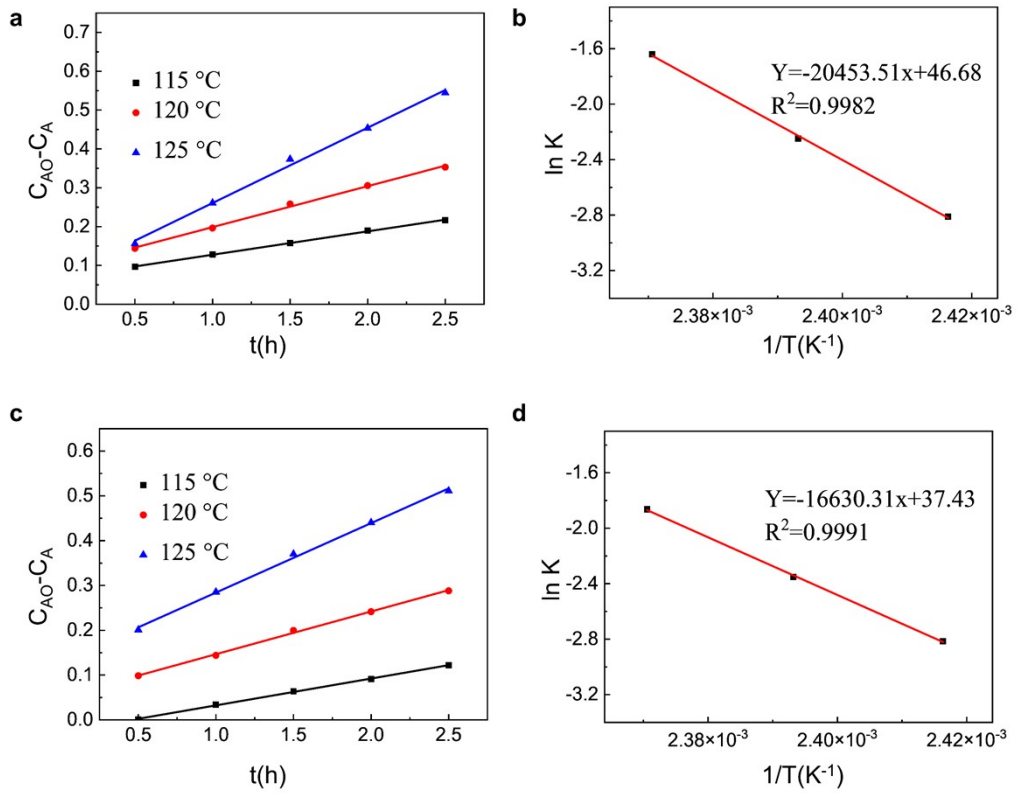

Figure S1. Pseudo-first-order fits for the oxidation of 1,2,3,4-tetrahydronaphthalene with O_2 catalyzed by T(4-Br)PPCo (a,b) and CoPor-PAF-4 (c,d).

Table S7. The pseudo-first-order kinetic parameters in oxidation of 1,2,3,4-tetrahydronaphthalene[a].

Entry	Catalysts	Temperature (°C)	k (h^{-1})	R^2	Ea (kJ/mol)
1	T(4-Br)PPCo	115	0.0602	0.9992	
2		120	0.1056	0.9974	170.1
3		125	0.1940	0.9961	
4	CoPor-PAF-4	115	0.0599	0.9991	
5		120	0.0953	0.9982	138.3
6		125	0.1551	0.9977	

[a] Glass reaction tube (25 mL), 1,2,3,4-tetrahydronaphthalene (10 mmol, 1.3221 g), O_2 (0.10 MPa), catalyst (1.0 mg), 600 rpm.

Table S8. Metal contents in CoPor-PAF-4 samples by ICP-OES.

Materials	Measured contents (wt %) Co
CoPor-PAF-4	1.76
Liquid phase	< 40 ppb

Table S9. Reusability for the catalytic oxidation of *p*-ethylnitrobenzene [a].

Run	Catalysts	Conversion (%)	Selectivity (%)		
			Ar_1-OOH	Ar_1-OH	Ar_1=O
1st	CoPor-PAF-4	**60.1**	**5.5**	**N. D.**	**94.5**
2nd	CoPor-PAF-4	58.6	6.3	**N. D.**	93.7
3rd	CoPor-PAF-4	54.8	7.5	**N. D.**	92.5

[a] *p*-ethylnitrobenzene (15.12 g, 100 mmol), O_2 (1.0 MPa), CoPor-PAF-4 (5.0 mg, 0.05 mg/mmol), 130 °C, 8.0 h, 600 rpm.

[b] No obvious product detected.

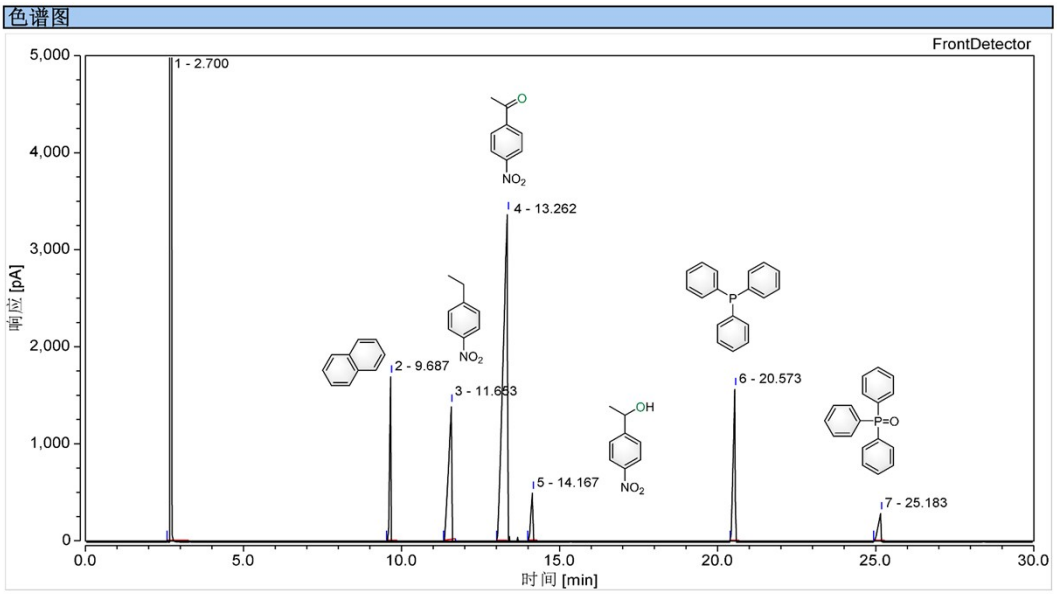

Figure S2. GC plot in oxidation of *p*-Ethylnitrobenzene

4. Effective Diffusion Coefficient

Estimation Method of Effective Diffusion Coefficient Using the Renkin Equation: in nanoconfined catalytic systems, the diffusion behavior of substrate molecules within pores is significantly influenced by the match between pore size and molecular dimensions. To quantitatively assess the mass transfer characteristics in the CoPor-PAF-4 catalyst, we employed the classical Renkin equation to estimate the effective diffusion coefficient (D_ϵ). This equation directly reflects the steric hindrance effect on diffusion caused by the ratio of molecular to pore size (λ/d_p). The detailed methodology is as follows:

4.1 Model Selection

Given that the pore size of CoPor-PAF-4 (d_p= 0.50–0.80 nm) is highly comparable to the kinetic diameter of substrate molecules ($\lambda \approx$ 0.58–0.72 nm), molecular diffusion within the pores is subject to strong steric hindrance, and its intrinsic pore diffusion coefficient (D_p) is much lower than the bulk diffusion coefficient (D_0). We used the Renkin equation to describe this restricted diffusion and considered the macroscopic structure of the porous medium to calculate the effective diffusion coefficient:

$$D_e = \frac{\epsilon_p}{\tau} \cdot D_p$$

$$\frac{D_p}{D_0} = \left(1 - \frac{\lambda}{d_p}\right)^2 \left[1 - 2.104\left(\frac{\lambda}{d_p}\right) + 2.09\left(\frac{\lambda}{d_p}\right)^3 - 0.95\left(\frac{\lambda}{d_p}\right)^5\right]$$

Where ϵ_p is porosity, τ is tortuosity, D_p is the restricted pore diffusion coefficient, D_0 is the bulk diffusion coefficient, λ is the kinetic diameter of the substrate molecule, and d_p is the characteristic pore size of the material.

4.2 Parameter Determination

(1) Porosity(ϵ_p) and tortuosity(τ)

The total pore volume of CoPor-PAF-4 measured by nitrogen physisorption is V_{pore} = 0.3701 $cm^3 \cdot g^{-1}$. Based on the typical skeletal density of similar porous aromatic frameworks ($\rho_{skeleton} \approx$ 2.0 $g \cdot cm^{-3}$), the porosity is calculated as:

$$\epsilon_p = \frac{V_{pore}}{V_{pore} + 1/\rho_{skeleton}} = \frac{0.3701}{0.3701 + 1/2} = 0.425$$

For amorphous porous materials, tortuosity typically ranges from 2 to 6. An intermediate value of τ = 3.5 is adopted as a reasonable estimate.

(2) Bulk Diffusion Coefficient (D_0)

The bulk diffusion coefficient of the substrate (taking *p*-ethylnitrobenzene as an example) in the free liquid phase was estimated using the Stokes-Einstein equation. At the reaction temperature of 130 °C (403 K), with liquid viscosity η = 0.4 cP = 4.0×10^{-4} Pa·s and hydrodynamic radius (related to kinetic diameter)r = $\lambda/2$ = 0.325 nm = 3.25×10^{-10} m:

Stokes-Einstein Equation

$$D_0 = \frac{k_B T}{6\pi\eta r} = \frac{1.38 \times 10^{-23} \times 403}{6\pi \times 0.0004 \times 3.25 \times 10^{-10}} \approx 2.3 \times 10^{-9} m^2/s$$

(3) Pore Size (d_p) and Molecular Kinetic Diameter (λ)

According to the NLDFT pore size distribution (Figure 4), the main pore sizes of CoPor-PAF-4 are 0.50, 0.68, 0.80 nm. The median value d_p = 0.68 nm is selected as the characteristic pore size for calculation. The kinetic diameter of *p*-ethylnitrobenzene is estimated as λ = 0.65 nm (based on molecular structure estimation and literature values).

(4) Ratio of Molecular to Pore Size (λ/d_p)

$$\frac{\lambda}{d_p} = \frac{0.65}{0.68} = 0.956$$

This ratio is very close to 1, indicating extremely strong confinement on molecular diffusion by the pore space.

4.3 Calculation and Results

(1) Calculation of Restricted Pore Diffusion Coefficient D_p

Substituting λ/d_p = 0.956 into the Renkin equation:

$$\frac{D_p}{D_0} = (1 - 0.956)^2\left[1 - 2.104(0.956) + 2.09(0.956)^3 - 0.95(0.956)^5\right]$$

The calculation yields:

$$\frac{D_p}{D_0} \approx 1.94 \times 10^{-4}$$

$$D_p = 2.3 \times 10^{-9} \times 1.94 \times 10^{-4} \approx 4.46 \times 10^{-13} m^2/s$$

(2) Calculation of Effective Diffusion Coefficient D_e

$$D_e = \frac{\epsilon_p}{\tau} \cdot D_p = \frac{0.425}{3.5} \times 4.46 \times 10^{-13} \approx 5.4 \times 10^{-14} m^2/s$$

4.4 Pore Size Sensitivity Analysis

To evaluate the impact of pore size distribution, calculations were performed for d_p = 0.50 nm and d_p = 0.80 nm separately:

(1) For d_p = 0.50 nm, λ/d_p = 1.3>1, the Renkin equation predicts that diffusion is almost completely inhibited ($D_p/D_0 \rightarrow 0$).

(2) For d_p = 0.80 nm, λ/d_p =0.81, the calculated $D_e \approx 3.2\times10^{-13}$ m^2/s

The value $D_e \approx 5.4\times10^{-14}$ m^2/s, obtained using the main pore size of 0.68 nm, represents the average diffusion level of the system. This value falls within the typical range for liquid-phase restricted diffusion in microporous materials (10^{-14}~10^{-16} m^2/s), validating the reasonableness of the estimation.

5. Weisz Modulus (∅)

In heterogeneous catalysis, the diffusion rate of reactants within catalyst particles directly affects the overall reaction efficiency. To quantitatively evaluate the extent of mass transfer limitations inside CoPor-PAF-4 catalyst particles, we introduce the Weisz modulus (∅) as a dimensionless criterion. Its core physical meaning is the ratio of the actually observed reaction rate inside the catalyst particle to the intrinsic reaction rate that would occur if diffusion were infinitely fast. When ∅ is significantly greater than 1, internal diffusion limitations are severe; when ∅ is much less than 1, the reaction is primarily controlled by intrinsic kinetics.

5.1 Definition and Formula of the Weisz Modulus

For spherical catalyst particles, the most commonly used expression for the Weisz modulus is:

$$\emptyset = \frac{r_{mass} \times \rho_{particle} \times R^2}{D_e \times C_s}$$

∅: Weisz modulus (dimensionless), quantifying the degree of internal diffusion influence.

r_{mass}: Measured reaction rate based on catalyst mass (unit: $mol \cdot kg^{-1} \cdot s^{-1}$)

$\rho_{particle}$: Catalyst particle density (including pores) (unit: $kg \cdot m^{-3}$)

R: Characteristic length of the catalyst particle (unit: m). For spherical particles,

typically the radius.
C_s: Reactant concentration surface of the catalyst particle (unit: mol·m^{-3}).

5.2 Parameter Acquisition and Calculation (Taking *p*-Ethylnitrobenzene as an Example)

(1) Mass-Based Reaction Rate r_{mass}: From the optimal conditions in **Table 3** (5 mg catalyst, 100 mmol substrate, 130 °C, 1.0 MPa O_2, 8 h, conversion 60.1%):

- Moles of substrate consumed: n = 100 mmol × 60.1% = 0.0601 mol
- Reaction time: t = 8 h = 28800 s
- Catalyst mass: m_{cat} = 5 mg = 5×10^{-6} kg
- Mass-based reaction rate**:**

$$r_{mass} = \frac{n}{m_{cat} \times t} = \frac{0.0601}{5 \times 10^{-6} \times 28800} \approx 0.417$$

(2) Catalyst Particle Density $\rho_{particle}$: Particle density can be calculated from the total pore volume and skeletal density:

- Total pore volume: V_{pore} = 0.3701 cm^3/g = 3.701×10^{-4} m^3/kg

$$\rho_{particle} = \frac{1}{V_{pore} + \frac{1}{\rho_{skeleton}}} = \frac{0.0601}{3.701 \times 10^{-4} + \frac{1}{2000}} \approx 1120$$

(3) Particle Characteristic Length R: SEM images (Figure 2) show CoPor-PAF-4 as spherical microspheres with diameters ranging from 0.5 to 1.0 μm. Take radius R = 0.25 μm = 2.5 × 10^{-7} m as a conservative estimate.

(4) External Surface Reactant Concentration C_s: *p*-ethylnitrobenzene is liquid at 130 °C, with density ~1200 kg·m^{-3} and molecular weight 151.16 g·mol^{-1}:

$$C_s \approx \frac{1200}{0.15116} \approx 7940$$

(5) Weisz Modulus Calculation

$$\emptyset = \frac{0.417 \times 1120 \times (2.5 \times 10^{-7})^2}{5.41 \times 10^{-14} \times 7940} \approx 0.068$$

5.3 Result Analysis and Validation

(1) Weisz Modulus Calculation Result
The calculated $\emptyset \approx 0.068$ nm is much less than 1, indicating that internal diffusion

limitations are very slight within the CoPor-PAF-4 catalyst particles, and the reaction is primarily controlled by intrinsic kinetics.

(2) Parameter Sensitivity Analysis

- Particle size effect: If a larger particle radius $R = 0.5\ \mu$m is taken, $\emptyset \approx 0.27$, still less than 1.
- Diffusion coefficient effect: Using a more conservative diffusion coefficient (considering stronger restriction from 0.50 nm pores), $\emptyset$ might increase to 0.2-0.4 range, but remains in the same order of magnitude.
- Concentration effect: Considering local decrease of surface concentration during reaction, C_s might be slightly lower than calculated, but would not significantly change the conclusion that $\emptyset \ll 1$.

6. Evaluation of Green Chemistry Metrics

6.1 Atom Economy (AE)

$$AE\% = \left(\frac{MW_{Product}}{\sum MW_{Reactants}}\right) \times 100\%$$

This is a theoretical maximum metric based on the stoichiometry of the chemical equation, assuming 100% yield and no by-products. It measures the intrinsic efficiency of a reaction route in terms of atom utilization.

6.2 Turnover Number (TON)

$$TON = \left(\frac{Moles_{product}}{Mass_{Catalytic\ Active\ Sites}}\right)$$

Measures the total productivity of a catalyst before its deactivation, reflecting catalyst durability and efficiency.

6.3 Turnover Frequency (TOF)

$$TOF = \frac{TON}{Time(h)}$$

6.4 Environmental Factor (E-factor)

$$E\text{-}factor = \left(\frac{Mass_{Total\ Waste}}{Mass_{Product}}\right)$$

Total Waste Mass = Total mass of all input materials - Mass of the product.

6.5 Reaction Mass Efficiency (RME)

$$RME\% = \left(\frac{Mass_{Product}}{\sum Mass_{All\ Input\ Materials}}\right) \times 100\%$$

This is a practical process metric. It accounts for stoichiometry, actual yield, excess reagents, and the mass of other materials like solvents and catalysts.

7. Experimental spectra

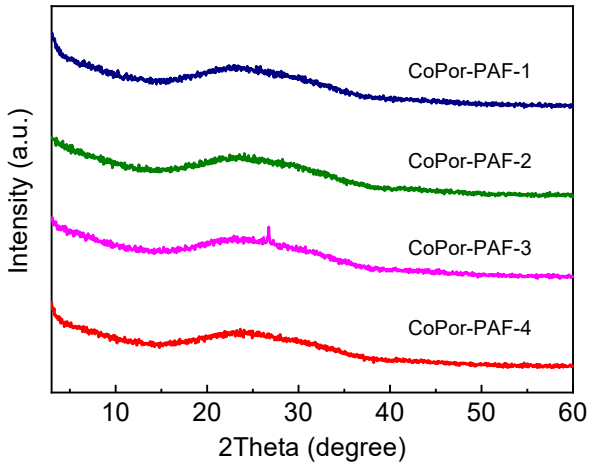

Figure S3. PXRD patterns of the synthesized CoPor-PAFs.

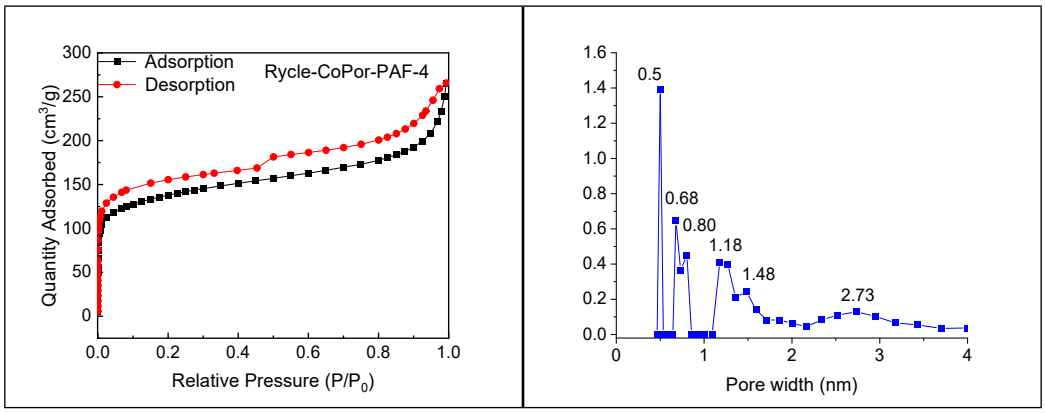

Figure S4. Nitrogen adsorption-desorption isotherms (insets) and corresponding pore width distributions of Rycle-CoPor-PAF-4.

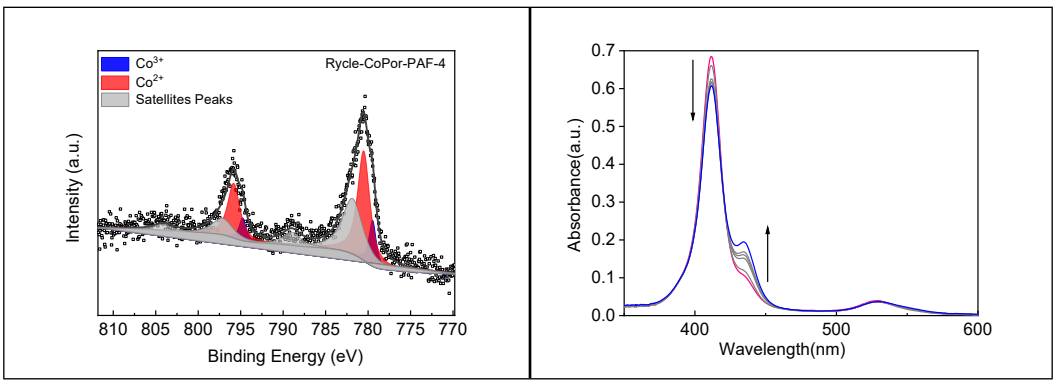

Figure S5. High-resolution narrow XPS scans of Rycle-CoPor-PAF-4 and UV-Vis Absorption Spectrum of T(4-Br)PPCo under Oxygen Atmosphere.

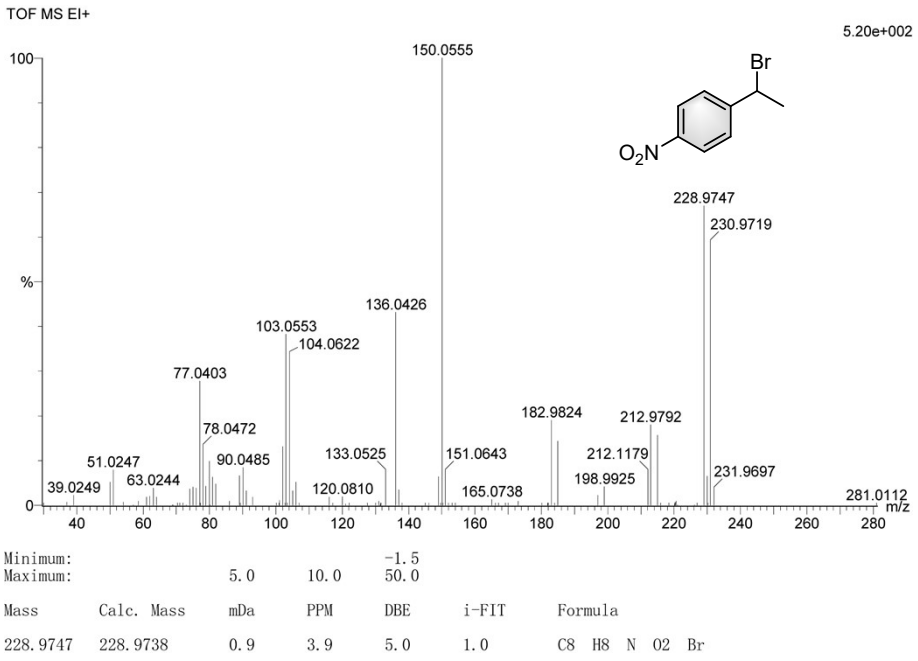

Figure S6. GC-MS spectra of quenching experiment in oxidation of α-C-H bonds in alkyl aromatics employing 1-ethyl-4-nitrobenzene as model substrate and $CBrCl_3$ as quenching reagent-1.

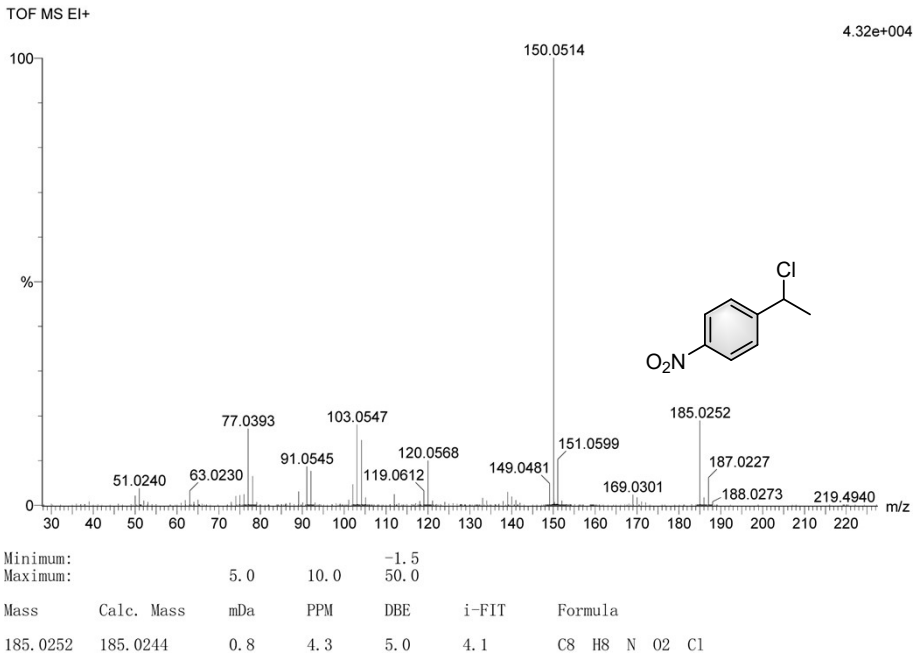

Figure S7. GC-MS spectra of quenching experiment in oxidation of α-C-H bonds in alkyl aromatics employing 1-ethyl-4-nitrobenzene as model substrate and $CBrCl_3$ as quenching reagent-2.

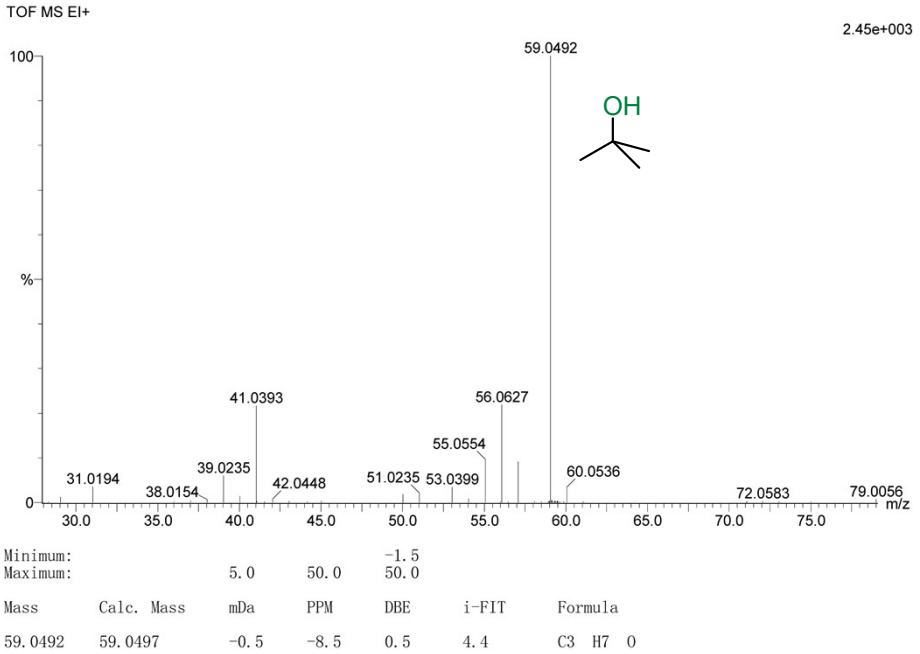

Figure S8. GC-MS spectra of quenching experiment in oxidation of α-C-H bonds in alkyl aromatics employing 1-ethyl-4-nitrobenzene as model substrate and $(CH_3)_3CBr$ as quenching reagent-2.

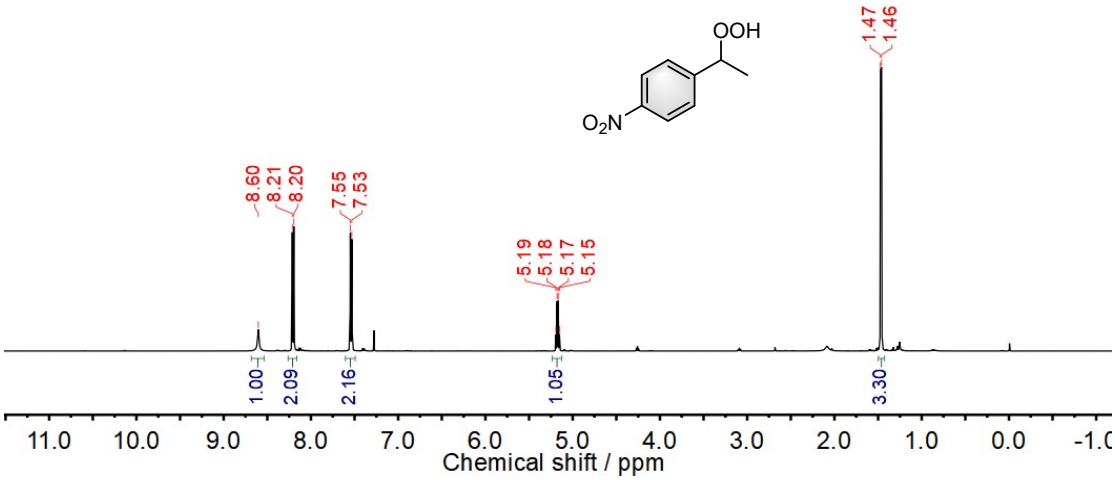

Figure S9. ^{1}H NMR spectrum of hydroperoxide in oxidation of 1-ethyl-4-nitrobenzene.

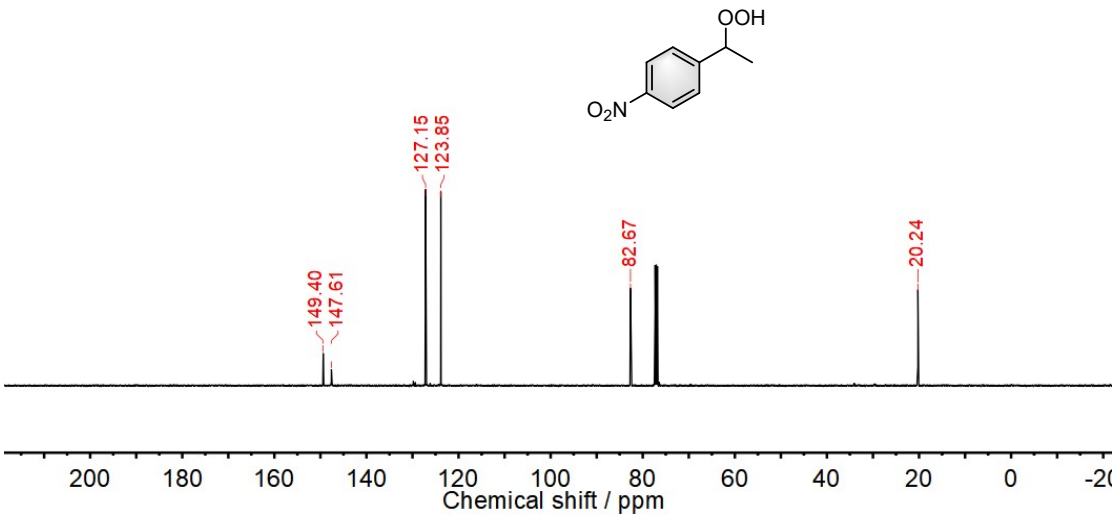

Figure S10. ^{13}C NMR spectrum of hydroperoxide in oxidation of 1-ethyl-4-nitrobenzene.

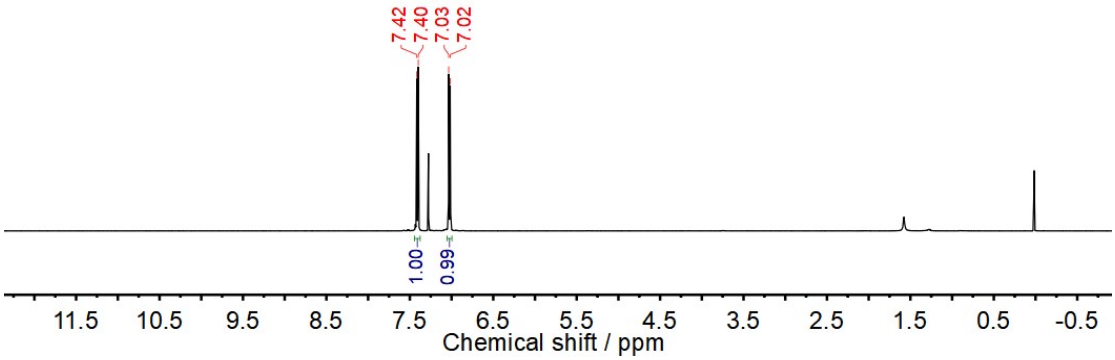

Figure S11. ^{1}H NMR spectrum of tetrakis(4-bromophenyl)methane.

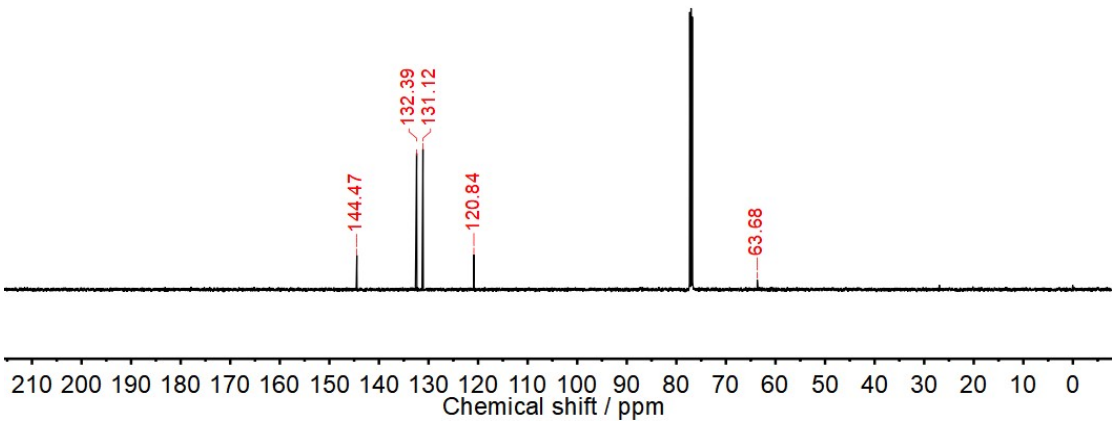

Figure S12. ^{13}C NMR spectrum of tetrakis(4-bromophenyl)methane.

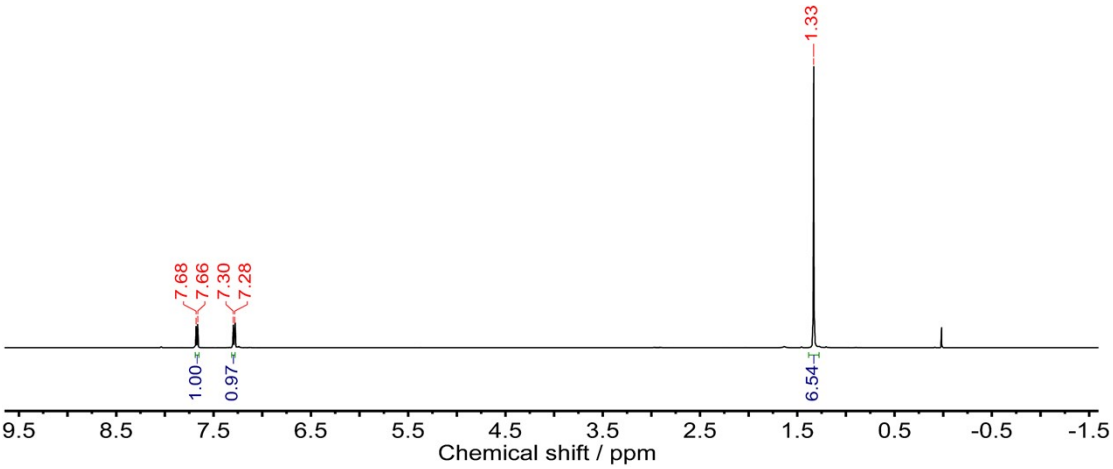

Figure S13. [1]H NMR spectrum of tetrakis(4-(4',4',5',5'-tetramethyl-1',3',2'-dioxaborolan-2'-yl)phenyl)methane.

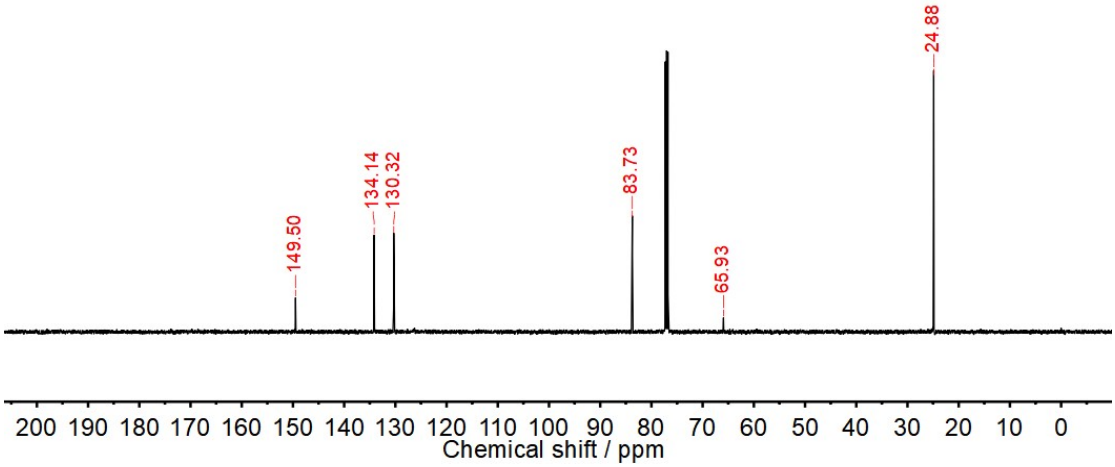

Figure S14. [13]C NMR spectrum of tetrakis(4-(4',4',5',5'-tetramethyl-1',3',2'-dioxaborolan-2'-yl)phenyl)methane.

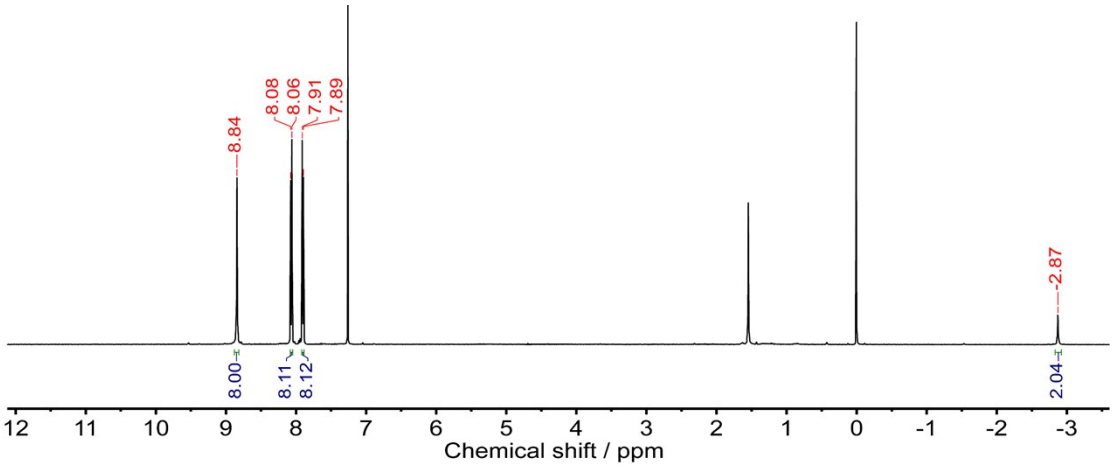

Figure S15. [1]H NMR spectrum of tetrakis(4-bromophenyl)porphyrin.

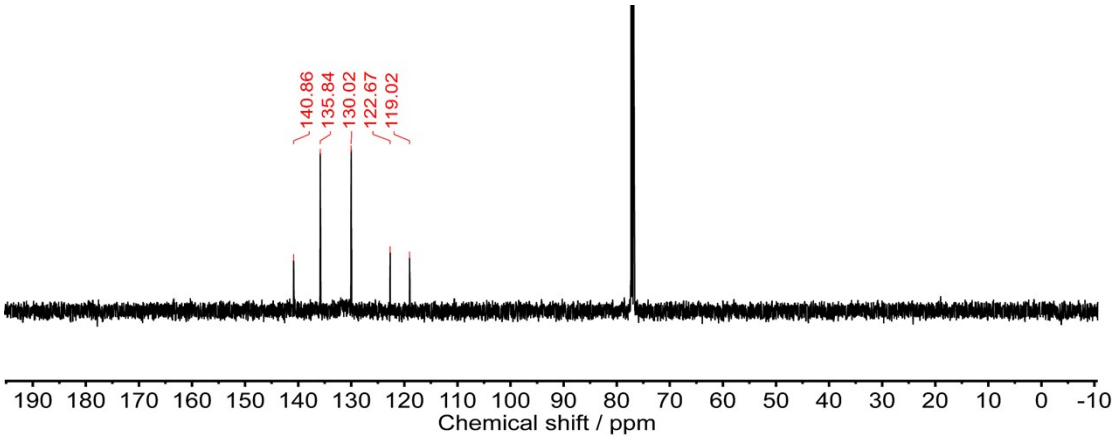

Figure S16. ^{13}C NMR spectrum of tetrakis(4-bromophenyl)porphyrin.

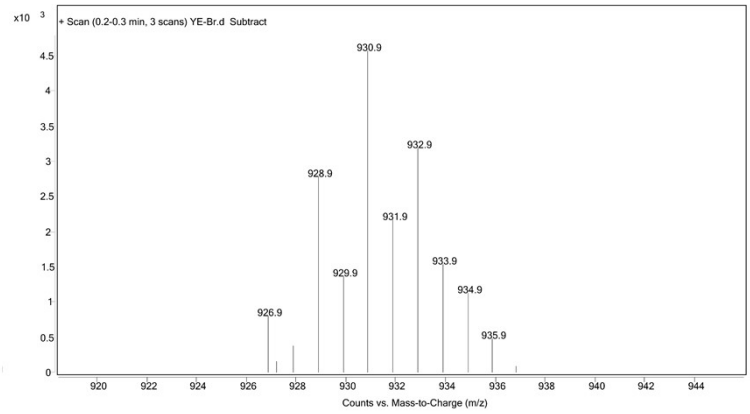

Figure S17. APCI-MS spectrum of tetrakis(4-bromophenyl)porphyrin.

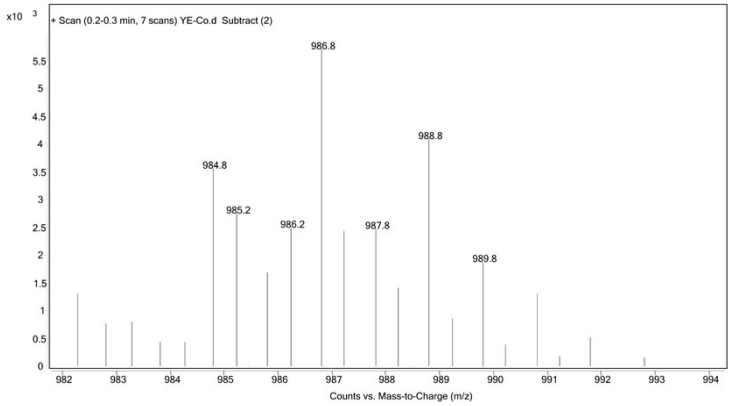

Figure S18. APCI-MS spectrum of tetrakis(4-bromophenyl)porphyrin Co.

8. References

[1] L. Zhu, D.P. Sheng, C. Xu, X. Dai, M.A. Silver, J. Li, P. Li, Y.X. Wang, Y.L. Wang, L.H. Chen, C.L. Xiao, J. Chen, R.H. Zhou, C. Zhang, O.K. Farha, Z.F. Chai, T.E. Albrecht-Schmitt, S. Wang, Identifying the Recognition Site for Selective Trapping of $^{99}TcO_4^-$ in a Hydrolytically Stable and Radiation Resistant Cationic Metal-Organic Framework, J. Am. Chem. Soc. 139 (2017) 14873-14876.

[2] D.P. Sheng, L. Zhu, C. Xu, C.L. Xiao, Y.L. Wang, Y.X. Wang, L.H. Chen, J. Diwu, J. Chen, Z.F. Chai, T.E. Albrecht-Schmitt, S.A. Wang, Efficient and Selective Uptake of TcO_4^- by a Cationic Metal-Organic Framework Material with Open Ag^+ Sites, Environ. Sci. Technol. 51 (2017) 3471-3479.

[3] L.A. Baldwin, J.W. Crowe, D.A. Pyles, P.L. McGrier, Metalation of a Mesoporous Three-Dimensional Covalent Organic Framework, J. Am. Chem. Soc. 138 (2016) 15134-15137.

[4] J.Q. Dong, Y. Liu, Y. Cui, Chiral porous organic frameworks for asymmetric heterogeneous catalysis and gas chromatographic separation, Chem. Commun. 50 (2014) 14949-14952.

[5] D.W. Feng, Z.Y. Gu, J.R. Li, H.L. Jiang, Z.W. Wei, H.C. Zhou, Zirconium-Metalloporphyrin PCN-222: Mesoporous Metal-Organic Frameworks with Ultrahigh Stability as Biomimetic Catalysts, Angew. Chem. Int. Edit. 51 (2012) 10307-10310.

[6] D.W. Feng, W.C. Chung, Z.W. Wei, Z.Y. Gu, H.L. Jiang, Y.P. Chen, D.J. Darensbourg, H.C. Zhou, Construction of Ultrastable Porphyrin Zr Metal-Organic Frameworks through Linker Elimination, J. Am. Chem. Soc. 135 (2013) 17105-17110.